Catenary-based visual servoing for tethered robots

Matheus Laranjeira, Claire Dune, Vincent Hugel

Catenary-based Visual Servoing for Tethered Robots

Matheus Laranjeira [1], Claire Dune[1] and Vincent Hugel[1]

***Abstract*— Tethers are used to supply power and transfer data for teleoperated robots. They are known to limit the robot's workspace and could have the effect of hampering its motion. What if we could take advantage of the tether? In this paper a new visual servoing scheme for catenary shaped deformable objects is introduced in order to control the tether parametric shape by properly moving its fixation point. In most of the visual servoing approaches the target object is rigid and distant from the controlled robot. On the contrary, in this paper, the object is deformable and attached to the robot, thus its 3D shape changes while the robot is moving. The experimental system is composed of two terrestrial mobile robots of the same motion capabilities linked with a slack rope. Simulation and real experiments validate the proposed control scheme for proper tether handling.**

I. Introduction

Tethered and umbilical systems are used to provide power, communication and assistance to robots operating in severe environments. Some planetary rovers are connected to a remote station by a cable to secure the exploration of unknown and steep terrains. Their motion can be controlled thanks to cameras that can be mounted either on the rover [1] or on the station [2]. Tethered systems are also designed for underwater missions. The underwater tether is usually slack, and links a remote operated vehicle (ROV) to a ship on the surface. Some research studies deal with solutions to prevent the ROV from beeing disturbed by the tether due to ship motion [3].

Long flexible sagging objects like tethers, cables, wires, hoses can be modeled by splines [4] and catenaries [5], [6], in the context of object transportation and aerial systems, or by parabolas [7], in the case of cable-driven parallel robots. These objects are subject to gravity and the geometrical equation that matches their shape can be used to control the motion of the load to be transferred from one location to another.

Visual servoing [8], [9] controls a robot motion to regulate some visual features that are usually extracted from rigid objects that can be fixed or moving freely. First, geometrical features such as points, line segments and circles were investigated [10]. Then, 3D models were introduced for known manufactured objects [11], [12], image moments to deal with objects of natural shape [13], splines for shape tracking [14] and algebraic curves for shape alignment [15]. Articulated objects were also considered [16]. Some recent works focus on deformable object shape control where robots push or pull the object to reach a desired configuration [17], [18]. In the context of hose transportation, several robots were attached to a semi-rigid cable and a coordinate visual servoing control was introduced based on the cable curvature derived from splines and GEDS (Geometrically Exact Dynamic Splines) [4]. Unknown deformable objects can be modeled thanks to their viscoelasticity properties [17] or using virtual geometrical features such as image points, distances and curvatures [18].

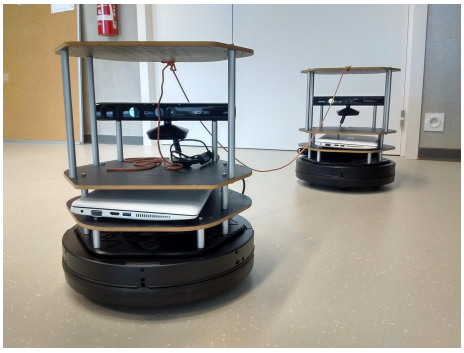

Fig. 1: Experimental setup: two Turtlebots [19] simulate a tether handling system for remotely operated robots. The leader robot freely explores its surroundings while the follower robot is expected to maintain the tether slack enough not to hamper the leader movements

This paper deals with a novel visual servoing strategy based on the deformable shape of a sagging tether that links two terrestrial mobile robots of the same motion capabilities. The objective is to free the leader robot from tether management while the follower robot will be able to position itself to ensure an average sag of the tether and proper orientation with respect to it. The three points below illustrate the contribution of this work:

- The tether is managed between two mobile robots through a visual system embedded on the follower robot that can extract visual information on the tether.
- The tether is modeled by a catenary shape whose parameters are estimated thanks to a real time curve fitting in the image. This allows to take into account the deformation of the tether beyond pixels detected in the image.
- An interaction matrix based on the estimated catenary parameters is calculated and used for the motion control of the follower robot with respect to the deformable tether.

The paper is organized as follows: Section II presents the tether modeling, Section III focuses on the visual servoing strategy used for controlling the position of the follower

[1] Cosmer Laboratory EA 7398, University of Toulon, France

robot with respect to the tether. Section IV presents and discusses the experimental results. Finally, Section V concludes the paper and gives directions for future work.

II. Tether modeling

A. Catenary-based geometrical modeling

The experimental set up is presented in Fig. 1. Two terrestrial mobile robots of the same motion capabilities simulate a tether handling system for remotely operated robots. The leader robot freely explores its surroundings while the follower robot is expected to maintain the tether slack enough not to hamper the leader movements. Figure 2 defines the notations and reference frames used in the remainder of the paper. Let Σ_{r_1} and Σ_{r_2} be two Cartesian frames centered at the middle of the robots wheel axis with X-axis pointing towards the front of the robot and a vertical Z-axis. A camera is mounted on the follower robot to track the tether shape. Let Σ_c be a Cartesian frame attached to the camera's optical center, with Z-axis being its optical axis and Y-axis vertically set towards the ground. It is assumed that the optical axis is aligned with the robot X-axis. A 3 millimeter orange rope that links the two robots simulates the tether. Its attachment points are at the same height and define the centers of the Cartesian frames Σ_1 and Σ_2, their orientation being the same as the robot they are attached to. The tether is modeled as a catenary, where R is its half-length, D is the half-span between the attachment points and H is the rope sag. Let Σ_0 be a Cartesian frame attached to the rope. Its center is the center of the rope and the X-axis and Z-axis are in the rope plane.

The classic equation of a catenary, expressed in frame Σ_0, has the following form [20]:

$$\Sigma_0 : \begin{cases} Y = 0 \\ Z = \frac{1}{C}\left[\cosh(Ct) - 1\right] \end{cases} \tag{1}$$

where $C = \frac{2 \cdot H}{R^2 - H^2}$. Expressing the same equation in Σ_2 leads to:

$$\Sigma_2 : \begin{cases} Y = \tan\theta X \\ Z = \frac{1}{C}\left[\cosh\left(C\left(\frac{Y}{\sin\theta} - D\right)\right) - 1\right] - H \end{cases} \tag{2}$$

where θ is the angle between the catenary plane and the Σ_2 X-axis. Finally, the same equation can be written in the camera frame (Σ_c) as:

$$\Sigma_c : \begin{cases} Y = -\frac{1}{C}\left[\cosh\left(C\left(\eta - D\right)\right) - 1\right] + H + Y_2 \\ Z = \cot\theta\left(-X + X_2\right) + Z_2 \end{cases} \tag{3}$$

where $\eta = \frac{-X + X_2}{\sin\theta}$ and (X_2, Y_2, Z_2) are the coordinates of Σ_2 in frame Σ_c.

A 3-D point with coordinates $P = (X, Y, Z)$ in the camera frame is projected on the image plane as a 2-D point with coordinates $p = (x, y)$ through the equation:

$$\begin{bmatrix} x \\ y \\ 1 \end{bmatrix} = \frac{1}{Z} \begin{bmatrix} f & 0 & c_x & 0 \\ 0 & f & c_y & 0 \\ 0 & 0 & 1 & 0 \end{bmatrix} \begin{bmatrix} X \\ Y \\ Z \\ 1 \end{bmatrix} \tag{4}$$

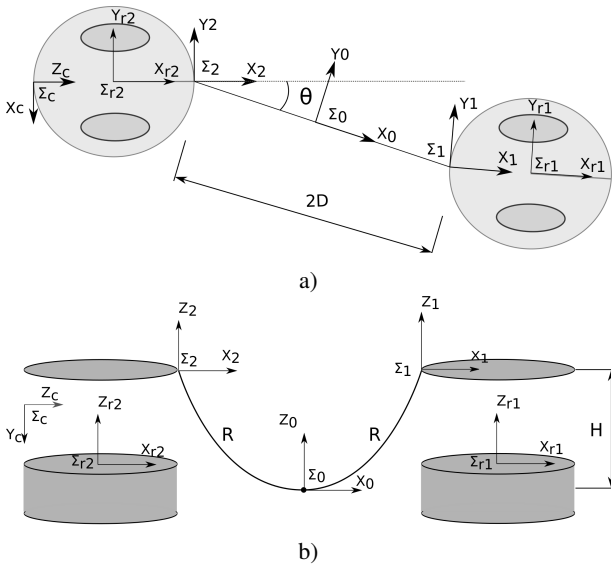

Fig. 2: Scheme of experimental set up. Two terrestrial mobile robots with 2-DOF (rotation and translation) are linked by a passive tether. (a) top view and (b) side view of the scene

where (c_x, c_y) are the coordinates of the principal point and f is the focal length [21]. Therefore, using Eqs. (3) and (4) we obtain the catenary projection on the image plane:

$$y = \eta_1 \left[-\frac{1}{C}\left(cosh\left(C\left(\eta_2 - D\right)\right) - 1\right) + aH_{max} + Y_2\right] \tag{5}$$

where

$$\eta_1 = \frac{b + \sqrt{1 - b^2}x}{\sqrt{1 - b^2}X_2 + bZ_2} \text{ and } \eta_2 = \frac{X_2 - Z_2 x}{b + x\sqrt{1 - b^2}}$$

As variable shape parameters for the projected curve in the image, we choose:

$$a = \frac{H}{H_{max}} \tag{6}$$

and

$$b = \sin\theta \tag{7}$$

with H_{max} being the tether maximum acceptable sag (i.e. the tether attachment point height). The parameters a and b are respectively relative to the tether slackness and orientation with respect to the follower robot. They range in the interval $[0, 1]$, and the sign of $\sin\theta$ is discriminated by the side on which the tether appears in the image. The tether is horizontal when $a = 0$ and it reaches the ground when $a = 1$. When $b = 0$ the tether belongs to the plane (Σ_2, X_2, Z_2) and when $b = 1$ it belongs to the plane (Σ_2, Y_2, Z_2).

III. Visual servoing algorithm

In this paper, the tether 3D shape is defined by the following feature vector:

$$\mathbf{s} = (a, b)$$

where a and b were defined in Eq. (6) and (7). The algorithm is depicted on Fig. 3, and is composed of three main steps that are detailed below.

$$\begin{cases} \frac{\partial y(x_i,\mathbf{s})}{\partial a} = \frac{\eta_1}{C}\left[\frac{1}{C}\frac{\partial C}{\partial a}\left(\cosh\left(C\eta_2 - CD\right) - 1\right) - \sinh\left(C\eta_2 - CD\right)\left(A_1 + A_2 + A_3\right) + H_{max}\right] \\ \frac{\partial y(x_i,\mathbf{s})}{\partial b} = -\frac{1}{C}\frac{\partial \eta_1}{\partial b}\left[\cosh\left(C\eta_2 - CD\right) - 1 - C\left(H + Y_2\right)\right] - \eta_1 \frac{\partial \eta_2}{\partial b}\sinh\left(C\eta_2 - CD\right) \end{cases} \tag{8}$$

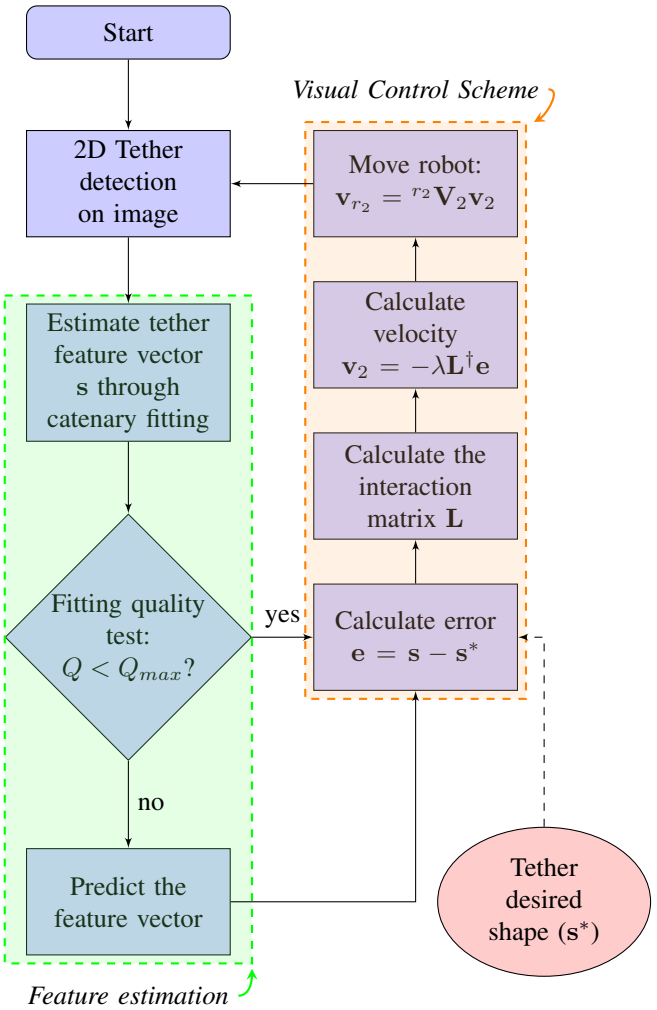

Fig. 3: Algorithm chart flow for catenary-based visual servoing of tethered robots

A. Tether detection

The first step deals with the tether detection in the image. It is assumed that the tether has a characteristic color in order to use color segmentation. Knowing that the tether attachment point to the follower robot is above the camera, the detection of pixels belonging to the tether starts in a rectangular region of interest (ROI) in the middle top of the image and iteratively follows the tether shape with a sequence of squares ROIs (Fig. 4a). The location of a subsequent ROI is calculated from the pixel average coordinates of the tether end in the previous ROI. The transformation from pixel to metric coordinates in the image plane is given in Eq. (4).

Wrong rope detection may occur due to lighting changes or when the tether cannot be distinguished from background objects of similar color. A minimum number of detected points and a Pearson coefficient threshold are used to validate the tether detection. The cases of wrong detection are treated with a linear feature prediction as is explained in the next subsection.

B. Estimation of tether shape features

The feature vector is estimated through a non-linear least-square fitting procedure based on a Gauss-Newton algorithm. The following objective function is minimized during the fitting process:

$$\chi^2 = \sum_{i=1}^{N} r_i^2(\mathbf{s}) \tag{9}$$

where $r_i\left(\mathbf{s}\right) = y_i - y(x_i, \mathbf{s})$ is the residual, (x_i, y_i) are the metric coordinates of the i-th detected point of the tether in the image, N is the total number of detected points and $y(x, \mathbf{s})$ is obtained from the current catenary projection in the image (Eq. (5)). The feature vector is iteratively estimated as follows:

$$\mathbf{s}^{k+1} = \mathbf{s}^k - \kappa\mathbf{J}_r^{\dagger}\mathbf{r}\left(\mathbf{s}^k\right)$$

where $\kappa \in \mathbb{R}^+$, $\mathbf{r}\left(\mathbf{s}^k\right)$ is a column vector that stacks the residuals $r_i\left(\mathbf{s}^k\right)$ and $\mathbf{J}_r^{\dagger}$ is the Moore-Penrose pseudo-inverse of the Jacobian matrix $\mathbf{J}_r = \frac{\delta \mathbf{r}}{\delta \mathbf{s}}$, whose i-th row has the following form:

$$\mathbf{J}_r\left(i\right) = \begin{bmatrix} -\frac{\partial y(x_i,\mathbf{s})}{\partial a} & -\frac{\partial y(x_i,\mathbf{s})}{\partial b} \end{bmatrix}$$

The partial derivatives are given in Eq. (8), with $A_1 = \eta_2\frac{\partial C}{\partial a}$, $A_2 = -D\frac{\partial C}{\partial a}$ and $A_3 = \frac{-A_2 + (CR)^2}{a\sqrt{(CR)^2 + 2CH}}$. The variables η_1, η_2, C, D, H, R and Y_2 are defined in Section II.

The proposed fitting procedure is not suited for small values of parameter $b = \sin\theta$. In such cases, the tether plane is too close to the camera axis, a region where the curve issued from catenary is degenerated and the sum of residuals (Eq. (9)) is no more selective enough. A possible solution to fit smaller values of b would be to use a parabola model $y = f_p(x)$ and to process the fitting using its inverse function relative to the first half of the parabola projection ($x = f_p^{-1}(y)$). Another solution would be to add an extra camera such that the tether plane is never parallel to both camera's axes.

The fitting algorithm was tested in simulation and on real images. As a result, the estimation of $\mathbf{s}$ is exploitable as soon as 30% of the tether is detected. In Fig. 4, the detection finds 70% of the tether, which allows an accurate fitting. The fitting quality is evaluated by the index $Q = \frac{\chi^2}{N}$. For values higher than a empirically tuned threshold, the estimated features are not used in the control velocity calculation. Instead, a first order linearization of Eq. (11) is used to predict the feature vector value, as follows:

$$\mathbf{s}(t + dt) = \mathbf{s}(t) + \mathbf{L}(t)\mathbf{v}_2(t) \tag{10}$$

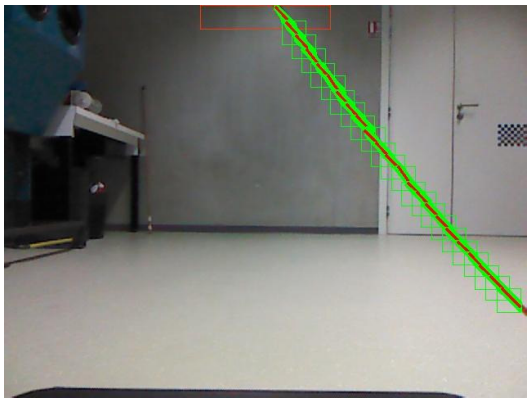

a)

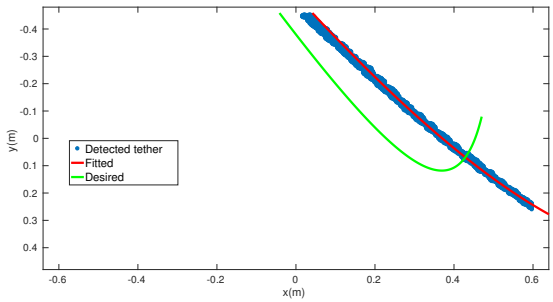

b)

Fig. 4: Catenary features estimation through a non-linear least-squares fitting. (a) tether detection in the robot image view. (b) tether fitting corresponding to the image view above. The rope detected points are in blue, the fitted and desired catenary curve are in red and green, respectively

where dt is the sampling period, $\mathbf{L}$ is the catenary interaction matrix and $\mathbf{v}_2 = (v_2, \omega_2)$ is the velocity vector of frame Σ_2 with linear velocity v_2 and angular velocity ω_2. In the current implementation, the number of consecutive iterations used for prediction is not limited.

C. Visual-based control scheme

The relation between the tether features time-derivative and the attachment point Σ_2 motion is given by the following equation:

$$\dot{\mathbf{s}} = \mathbf{L}\mathbf{v}_2 \tag{11}$$

The aim of visual-based control schemes is to minimize the error $\mathbf{e}$ defined as

$$\mathbf{e} = \mathbf{s} - \mathbf{s}^* \tag{12}$$

where $\mathbf{s}$ and $\mathbf{s}^*$ are respectively the current and desired feature vectors (see Fig. 4). In order to ensure an exponential decay of the error, the following control law is designed [8]:

$$\mathbf{v}_2 = -\lambda \mathbf{L}^\dagger \mathbf{e} \tag{13}$$

where $\mathbf{L}^\dagger$ is the Moore-Penrose pseudo-inverse of $\mathbf{L}$ and $\lambda \in \mathbb{R}^+$. The velocity of the follower robot is then obtained through: $\mathbf{v}_{r_2} = {}^{r_2}\mathbf{V}_2 \mathbf{v}_2$, where ${}^{r_2}\mathbf{V}_2$ is the twist transformation matrix from frame Σ_2 to frame Σ_{r_2}.

We used a nonholonomic robot with 2 DOF to experimentally validate our control scheme, as is explained in Section IV. In such case, the conversion between $\mathbf{v}_{r_2}$ and the pair of control variables $\mathbf{u} = (v_x, \omega_z)$ is achieved by the following projection:

$$\mathbf{u} = \begin{bmatrix} 1 & 0 & 0 & 0 & 0 & 0 \\ 0 & 0 & 0 & 0 & 0 & 1 \end{bmatrix} \mathbf{v}_{r_2}$$

D. Interaction matrix computation

The interaction matrix $\mathbf{L}$ is the tether deformation model. It links the relative motion of the attached points to the derivative of the tether parameters. Contrary to [18], the object has a known parametric shape and this matrix is analytically computed from the definition of $\mathbf{s} = (\mathbf{a}, \mathbf{b})$.

Let $P_0 = (X_0, Y_0, Z_0)$ and $P_1 = (X_1, Y_1, Z_1)$ be the centers of frames Σ_0 and Σ_1, respectively. Evaluating and differentiating Eq. (2) at P_1, we get

$$\dot{H} = -\frac{\dot{C}}{C^2}\left[\cosh(CD) - 1\right] + \sinh(CD)\left(\frac{\dot{C}D}{C} + \dot{D}\right) \tag{14}$$

and differentiating the expression of C in Eq. (1) we have

$$\dot{C} = K_C \dot{H} \tag{15}$$

where $K_C = -\frac{2\left(R^2+H^2\right)}{\left(R^2-H^2\right)^2}$. Then, from the definition of a in Eq. (6) and replacing Eq. (15) in (14), we obtain

$$\dot{a} = \frac{K_H}{H_{max}} \dot{D} \tag{16}$$

where

$$K_H = \frac{sinh(CD)}{1 + \frac{K_C}{C^2}\left[\cosh(CD) - 1 - CD\sinh(CD)\right]}$$

The relative motion of P_1 in the reference frame Σ_2, due to the velocity of the follower robot $\mathbf{v}_2$ expressed in Σ_2 is:

$$\dot{P}_1 = -v_2 - \omega_2 \times P_1 \tag{17}$$

Geometrically,

$$\dot{P}_0 = \frac{\dot{P}_1}{2} \tag{18}$$

and

$$\dot{D} = \frac{X_0\dot{X}_0 + Y_0\dot{Y}_0}{D} \tag{19}$$

Thus, using Eqs. (17) and (18) in (19) we have:

$$\dot{D} = \frac{1}{2}\begin{bmatrix} -\cos\theta \\ -\sin\theta \\ 0 \\ Z_1\sin\theta \\ -Z_1\cos\theta \\ Y_1\cos\theta - X_1\sin\theta \end{bmatrix}^\top \mathbf{v}_2 \tag{20}$$

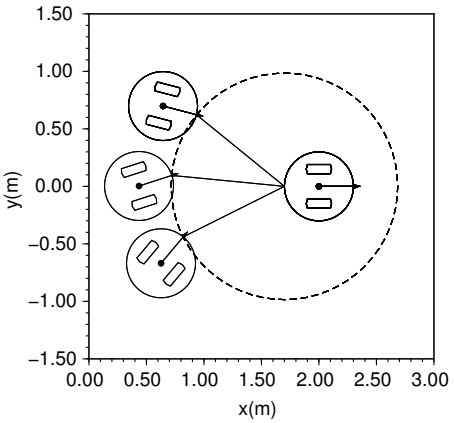

Fig. 5: Multiple positions of the follower robot for the same tether slackness and orientation: the problem only constrains the tether shape and orientation w.r.t. the follower robot

Finally, using Eq. (20) in (16) and given that $b = \sin\theta$,

$$\dot{a} = \frac{K_H}{2H_{max}} \begin{bmatrix} -\sqrt{1-b^2} \\ -b \\ 0 \\ Z_1 b \\ -Z_1\sqrt{1-b^2} \\ Y_1\sqrt{1-b^2} - X_1 b \end{bmatrix}^\top \mathbf{v}_2 \qquad (21)$$

Differentiating $b = \frac{Y_0}{D}$ leads to:

$$\dot{b} = \frac{\dot{Y}_0 - b\dot{D}}{D}$$

From the expressions of $\dot{Y}_0$ and $\dot{D}$ in Eqs. (18) and (20) respectively, we get:

$$\dot{b} = \frac{1}{2D} \begin{bmatrix} b\sqrt{1-b^2} \\ -1+b^2 \\ 0 \\ Z_1(1-b^2) \\ Z_1 b\sqrt{1-b^2} \\ -Y_1 b\sqrt{1-b^2} - X_1(1-b^2) \end{bmatrix}^\top \mathbf{v}_2 \qquad (22)$$

The complete interaction matrix (Eq. (23)) is composed of the rows given in Eqs. (21) and (22) with one more simplification: $Z_1 = 0$ since the attachment points are at the same height. The values of X_1 and Y_1 are geometrically calculated from Eq. (2).

The rank of L is 2, which means that this control law only commands two degrees of freedom of the follower robots, *i.e.* the relative attached points distance and the follower orientation with regards to the tether plane. Figure 5 shows several follower positions for the same set of parameters $s = (a, b)$. Remaining degrees of freedom are thus available for additional tasks, such as obstacle avoidance.

IV. Experimental results

A. Setup

One simulation and two real experiments are presented in order to validate the control law. Two Turtlebots [19] with 2 DOF (translation v_x and rotation w_z) are used as experimental robots. They are equipped with a Kinect device and linked by a 1.4 meter long and 3 millimeter thick orange rope (Fig. 1). The rope maximum sag is $H_{max} = 0.40$m, corresponding to its attachment point's height. The servoing algorithm runs in the follower robot computer, which is equipped with a Intel Core i5-2410M @ 2.3 GHz processor. The video frame rate is fixed to 10Hz. The same robot motion capabilities, rope length, thickness and maximum sag are used in simulation and real experiments.

B. Simulation

The objective of the simulation is that the follower robot moves the tether from a very slackened to a moderately tight shape. The tether orientation is controlled, passing from a large angle θ to a desired smaller angle. The initial and desired values of the feature vector are $\mathbf{s}_o = (0.9, 0.8)$ and $\mathbf{s}^* = (0.5, 0.5)$, respectively. We assume that the robots can perfectly estimate the tether parameters, so the fitting process is not simulated. Figure 6 presents the simulation results. As expected, both parameters have an exponential decay and converge to the desired value within 4 seconds for a gain $\lambda = 0.75$ and a sampling period of 0.1 seconds.

C. Real experiments

In the first experiment, the simulation initial conditions are repeated and the follower robot moves the tether from an initial shape $\mathbf{s}_o = (0.9, 0.8)$ to a desired shape $\mathbf{s}^* = (0.5, 0.5)$. We used the same gain as for simulation ($\lambda = 0.75$) and a fitting quality threshold $Q_{max} = 1$. Results are summarized in Fig. 7.

In the second experiment (Fig. 8), the leader robot is freely displaced while the follower robot ensures that the rope keeps a desired shape $\mathbf{s}^* = (0.7, -0.5)$. First, the leader robot moves forward, then turns left (24s). Next, it moves about 1.25 meters forward (38s), makes a half-turn (50s) and moves about 1.25 meters forward again (64s). At the end, it makes a quarter turn and moves about 0.50 meters backward (76s). Compared with the first experiment, a higher value was set to the tether first parameter in order to give more freedom of maneuvering to the leader robot. We used $Q_{max} = 1$ and two different gains for linear and angular velocities: $\lambda_l = 1.0$ and $\lambda_\omega = 6.0$, respectively (see discussion below). Figure 8c presents the fitting quality index evolution during the experiment. The feature prediction was used 20 times in cases of wrong rope detection and more 38 times due to inaccurate fitting.

In Fig. 7, the angular velocity command does not converge to zero, and remains quasi constant. This is due to the limitations of our experimental platform that cannot achieve a rotation velocity lower than 0.05 rad/s. In the second experiment, we selected a higher gain for the angular velocity compared to the linear velocity gain in order to overcome

$$\mathbf{L} = \begin{bmatrix} -\frac{K_H\sqrt{1-b^2}}{2H_{max}} & -\frac{K_H b}{2H_{max}} & 0 & 0 & 0 & \frac{K_H\left(Y_1\sqrt{1-b^2}-X_1 b\right)}{2H_{max}} \\ -\frac{b\sqrt{1-b^2}}{2D} & \frac{-1+b^2}{2D} & 0 & 0 & 0 & -\frac{Y_1 b\sqrt{1-b^2}+X_1(1-b^2)}{2D} \end{bmatrix} \tag{23}$$

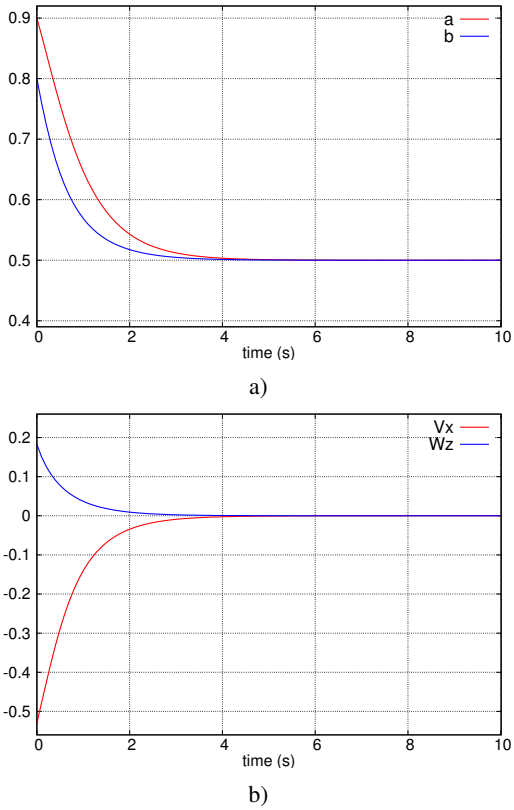

Fig. 6: Simulation results for tether shape control. (a) the parameters evolution. The tether goes from an initial to a desired shape ($\mathbf{s}_o = (0.9, 0.8)$ and $\mathbf{s}^* = (0.5, 0.5)$, respectively). (b) the control velocities. Linear velocity (v_x) in m/s and angular velocity (w_z) in rad/s

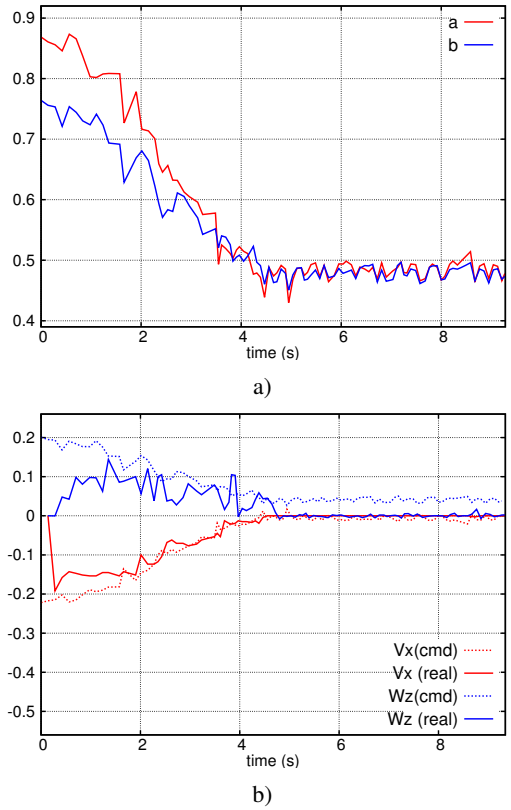

Fig. 7: Results of a real experiment for tether shape control. (a) the tether parameters evolution. The tether goes from an initial to a desired shape ($\mathbf{s}_o = (0.9, 0.8)$ and $\mathbf{s}^* = (0.5, 0.5)$, respectively). (b) the control velocities. Linear velocity (v_x) in m/s and angular velocity (w_z) in rad/s

this problem. As a future improvement, an integrator compensator to deal with the low level control of the velocity can be added to the servoing loop.

Looking at Fig. 7, we can note that the real experimentation curves are noisy compared with those obtained in simulation. This is mainly due to wrong rope detection that can affect the tether feature estimation. Another reason is the possible rope oscillation during the robot motion, which can occur when the robot halts and restarts motion. This could be taken into account by designing a dynamic controller that takes the rope inertia into account. In addition, the rope can be tracked in the image by a gradient-guided algorithm.

V. Conclusions and Perspectives

This paper presents a new visual servoing control scheme to manage a tether linking two terrestrial mobile robots. The tether is modeled by a catenary and its shape parameters are estimated by a non-linear least square fitting. A control law that takes into account the tether deformation was introduced in order to allow the robot to visually control the tether shape. The control scheme is validated by simulation and by two series of real experiments. The comparison of simulation and real experiments shows that both curves converge, validating the proposed control law. The vision-based tether shape controller implemented here gives promising results.

Future work will address the extension of the visual control scheme to multiple 6-D0F robots, and the use of complementary sensors to increase visual feature detection accuracy.

Acknowledgments

This work was achieved thanks to specific funding from the France PACA (Provence-Alpes-Cte-d'Azur) region, and the French SUBSEATECH company, located in Marseille, South-East of France (http://www.subsea-tech.com, pierre.marty@subsea-tech.com).

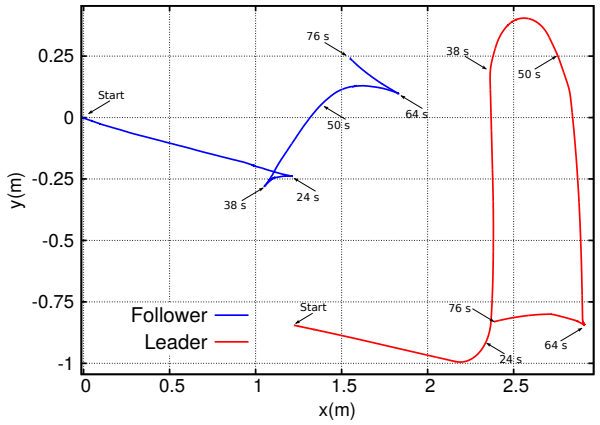

a)

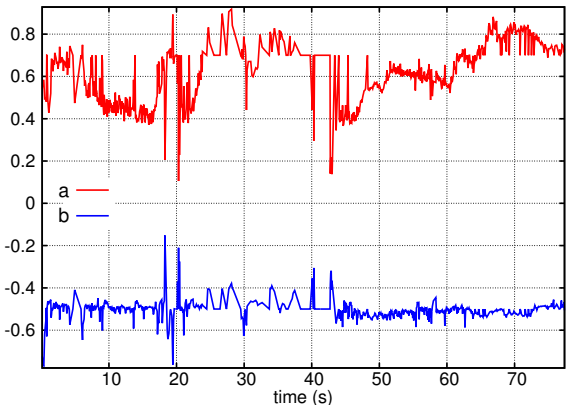

b)

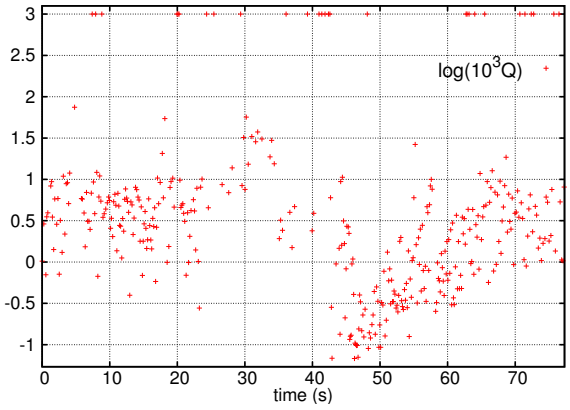

c)

Fig. 8: Two robots are linked by a tether. The leader robot freely moves while the follower robot maintains a desired tether shape $\mathbf{s}^* = (0.7, -0.5)$. (a) the leader and follower trajectories with time indications in seconds. (b) the tether parameters evolution. (c) the fitting quality index Q evolution during the experiment. Feature prediction is used in cases of wrong rope detection and inaccurate fitting ($Q = 1$ i.e. $log(10^3 Q) = 3$)

REFERENCES

[1] D. Tsai, I. A. D. Nesnas, and D. Zarzhitsky, "Autonomous vision-based tethered-assisted rover docking," in *2013 IEEE/RSJ International Conference on Intelligent Robots and Systems*, Nov 2013, pp. 2834–2841.

[2] J. Iqbal, S. Heikkila, and A. Halme, "Tether tracking and control of rosa robotic rover," in *Control, Automation, Robotics and Vision, 2008. ICARCV 2008. 10th International Conference on*, Dec 2008, pp. 689–693.

[3] S. Prabhakar and B. Buckham, "Dynamics modeling and control of a variable length remotely operated vehicle tether," in *Proceedings of OCEANS 2005 MTS/IEEE*, Sept 2005, pp. 1255–1262 Vol. 2.

[4] Z. Echegoyen, I. Villaverde, R. Moreno, M. Graa, and A. dAnjou, "Linked multi-component mobile robots: Modeling, simulation and control," *Robotics and Autonomous Systems*, vol. 58, no. 12, pp. 1292 – 1305, 2010, intelligent Robotics and Neuroscience. [Online]. Available: http://www.sciencedirect.com/science/article/pii/S0921889010001533

[5] J. Estevez and M. Graña, *Robust Control Tuning by PSO of Aerial Robots Hose Transportation*. Cham: Springer International Publishing, 2015, ch. Bioinspired Computation in Artificial Systems: International Work-Conference on the Interplay Between Natural and Artificial Computation, IWINAC 2015, Elche, Spain, June 1-5, 2015, Proceedings, Part II, pp. 291–300.

[6] T. Lee, "Geometric controls for a tethered quadrotor uav," in *2015 54th IEEE Conference on Decision and Control (CDC)*, Dec 2015, pp. 2749–2754.

[7] T. Dallej, M. Gouttefarde, N. Andreff, R. Dahmouche, and P. Martinet, "Vision-based modeling and control of large-dimension cable-driven parallel robots," in *2012 IEEE/RSJ International Conference on Intelligent Robots and Systems*, Oct 2012, pp. 1581–1586.

[8] F. Chaumette and S. Hutchinson, "Visual servo control. i. basic approaches," *IEEE Robotics Automation Magazine*, vol. 13, no. 4, pp. 82–90, Dec 2006.

[9] ——, "Visual servo control. ii. advanced approaches [tutorial]," *IEEE Robotics Automation Magazine*, vol. 14, no. 1, pp. 109–118, March 2007.

[10] B. Espiau, F. Chaumette, and P. Rives, "A new approach to visual servoing in robotics," *IEEE Transactions on Robotics and Automation*, vol. 8, no. 3, pp. 313–326, Jun 1992.

[11] A. Comport, E. Marchand, and F. Chaumette, "Robust model-based tracking for robot vision," in *IEEE/RSJ Int. Conf. on Intelligent Robots and Systems, IROS'04*, vol. 1, Sendai, Japan, September 2004, pp. 692–697.

[12] A. Petit, E. Marchand, and K. Kanani, "A robust model-based tracker for space applications: combining edge and color information," in *IEEE/RSJ Int. Conf. on Intelligent Robots and Systems, IROS'2013*, Tokyo, Japan, November 2013, pp. 3719–3724.

[13] O. Tahri and F. Chaumette, "Application of moment invariants to visual servoing," in *International Conference on Robotics and Automation*, vol. 3, 2003, pp. 4276–4281.

[14] P. Li, F. Chaumette, and O. Tahri, "A shape tracking algorithm for visual servoing," in *Proceedings of the 2005 IEEE International Conference on Robotics and Automation*, April 2005, pp. 2847–2852.

[15] A. Y. Yazicioglu, B. Calli, and M. Unel, "Image based visual servoing using algebraic curves applied to shape alignment," in *2009 IEEE/RSJ International Conference on Intelligent Robots and Systems*, Oct 2009, pp. 5444–5449.

[16] A. Comport, E. Marchand, and F. Chaumette, "Kinematic sets for real-time robust articulated object tracking," *Image and Vision Computing, IVC*, vol. 25, no. 3, pp. 374–391, March 2007.

[17] M. Higashimori, K. Yoshimoto, and M. Kaneko, "Active shaping of an unknown rheological object based on deformation decomposition into elasticity and plasticity," in *Robotics and Automation (ICRA), 2010 IEEE International Conference on*, May 2010, pp. 5120–5126.

[18] D. Navarro-Alarcon, Y.-h. Liu, J. G. Romero, and P. Li, "On the visual deformation servoing of compliant objects: Uncalibrated control methods and experiments," *The International Journal of Robotics Research*, vol. 33, no. 11, pp. 1462–1480, 2014.

[19] B. Gerkey and K. Conley, "Robot developer kits [ros topics]," *IEEE Robotics Automation Magazine*, vol. 18, no. 3, pp. 16–16, Sept 2011.

[20] J. Stewart, *Calculus*, 6th ed. Thomson Learning, 2007, ch. 7, p. 464.

[21] R. I. Hartley and A. Zisserman, *Multiple View Geometry in Computer Vision*, 2nd ed. Cambridge University Press, 2004, ch. 6, p. 155.